Research Square

Preprints are preliminary reports that have not undergone peer review.
They should not be considered conclusive, used to inform clinical practice,
or referenced by the media as validated information.

Gold bearing characteristics and fluid evolution of Arsenopyrite in Huanglong gold deposit, South Qinling Orogenic Belt

Zhongkai Xue
China University of Geosciences (Beijing)
Haoqing Huang
huanghhq999@163.com
Research Center of Applied Geology of China Geological Survey
Shukai Li
Anmin Xu
Xin Zheng
Baocheng Fan
Northwest University
Hang Li
You Guo
China University of Geosciences
Datong Liu

Article

Keywords: EPMA, Gold bearing characteristics, fluid evolution, Arsenopyrite, Huanglong gold deposit, South Qinling Orogenic Belt

Posted Date: February 27th, 2026

DOI: https://doi.org/10.21203/rs.3.rs-7841894/v1

License: This work is licensed under a Creative Commons Attribution 4.0 International License. Read Full License

Additional Declarations: No competing interests reported.

Abstract

To investigate the genesis of the Huanglong gold deposit, techniques such as electron probe microanalysis (EPMA) were employed to observe and analyze samples, with the aim of elucidating the occurrence state and formation environment of Au in the arsenopyrite—the principal gold-bearing mineral—and further exploring the genetic mechanisms. The birite porphyroblasts in the ore are categorized into fine, medium and coarse-grained types, corresponding to arsenopyrite crystal habits ranging from euhedral to anhedral. EPMA data indicate stable major element compositions in arsenopyrite, with Fe content ranging from 29.19% to 34.58%, S from 19.43% to 20.70%, and As from 45.13% to 46.21%. The empirical formula of arsenopyrite is derived as As 32.33 ~ 35.1, Fe 29.86 ~ 33.39, S 33.32 ~ 35.31. Scanning electron microscopy (SEM) observations revealed no native gold particles, suggesting that Au predominantly occurs as "invisible gold" within the arsenopyrite structure, likely through isomorphic substitution for S or As. The crystallization temperature of arsenopyrite is constrained between 360℃ and 475℃, indicating a high-temperature regime. The calculated sulfur fugacity (lgf(S2)) values range from − 10.5 to -6.6. The porous and fractured texture of arsenopyrite, coupled with the negative correlation between Au and S, points to characteristics of decompressive boiling. This process led to a decrease in sulfur fugacity within the hydrothermal system, triggering the decomposition and subsequent precipitation of Au complexes.

Introduction

The Shiquan-Hanyin gold metallogenic belt represents a prospective area for gold mineralization in the South Qinling region. Among the deposits within this belt, the Huanglong gold deposit is one of the most representative, with identified resources of approximately 5 tonnes. A detailed study of this deposit is therefore significant for guiding further exploration in the belt. Previous researchers have divided the structural fabric of the Huanglong deposit into four foliation stages, proposing that the S_2 foliation is closely associated with gold mineralization[1]. In-situ sulfur isotope analyses of gold-bearing minerals suggest mixed magmatic and crustal sources for the ore-forming materials. Fluid inclusion studies from mineralized quartz veins indicate that the ore-forming fluids were characterized by medium-low temperature, medium-low salinity, and low density, composed mainly of metamorphic water and meteoric water, with a minor magmatic component[2–3]. Pyrrhotite is identified as the principal gold-host mineral in the Huanglong deposit. Several studies on pyrrhotite-bearing sericite quartz schist and biotite-porphyroblast sericite-quartz schist ores, through major-trace element and sulfur isotope analyses, indicate that the pyrrhotite is predominantly of the monoclinic type, formed at relatively low temperatures consistent with fluid inclusion data[4]. These findings support a dominantly metamorphic-hydrothermal origin for the ore-forming fluids, with multi-source contributions to the metal budget. Garnet and biotite can serve as geothermometers to estimate regional thermal alteration temperatures. Previous work on garnet-biotite porphyroblast sericite quartz schist from the Jindoupo mining area yielded thermal alteration temperatures of 590℃-670℃, suggesting that thermal metamorphism played a key role in mobilizing Au[5].

In numerous gold deposits worldwide, gold exhibits a close association with sulfarsenide minerals, particularly arsenian pyrite, arsenopyrite, and loellingite. This relationship provides critical insights into the occurrence of gold and the mechanisms governing its mobilization and enrichment[6–7]. Studying the typomorphic characteristics of gold-host minerals in ores is essential for understanding the state of gold occurrence, its formation history, and the genetic model of the deposit[8–10] Arsenopyrite ($FeAs_{1.12}S_{1-x}$, $0 \le x \le 0.13$), which possesses a marcasite-derived structure, represents one of the principal gold-host minerals in mesothermal to epithermal hydrothermal deposits[11–12]. Although previous studies have conducted mineralogical investigations on pyrrhotite, biotite, and garnet in the region, no systematic research has been carried out on the widely developed arsenopyrite present in the carbonaceous biotite-porphyroblast sericite-quartz schist ores. Key questions regarding the genetic role of arsenopyrite in the Huanglong gold deposit and its specific implications for changes in the physicochemical conditions of the ore-forming fluids remain unresolved. This study focuses on arsenopyrite associated with pyrrhotite, employing mineralogical and mineral-chemical analyses to elucidate the genetic mechanisms of the Huanglong gold deposit.

The Qinling Orogenic Belt is divided from north to south by the Mianlve (SF1) and Shangdan (SF2) tectonic zones into the southern margin of the North China Block, the Qinling micro-block, and the northern margin of the Yangtze Block[13]. The northern Hanyin area is situated in the southern part of the South Qinling Indosinian fold-orogenic belt, along the northern continental margin of the Yangtze Block, within the Shiquan-Shenhe ductile décollement thrust nappe zone. It constitutes an important polymetallic metallogenic district in the South Qinling region (Fig. 1a). The area is predominantly underlain by Middle-Late Neoproterozoic Wudang Group and Yaolinghe Formation, as well as Early Paleozoic Cambrian, Ordovician, Silurian, and Late Paleozoic Devonian and Carboniferous sequences, comprising shallow-metamorphosed sedimentary clastic rocks, along with Cenozoic sediments. The region has undergone multiple tectonic episodes, resulting in the development of more than five NWW-EW trending brittle-ductile shear zones from north to south. These are characterized by tight isoclinal folds, intense shear deformation of quartz veins, and strong schistosity in rocks. Magmatic rocks exposed in the area are mainly Indosinian intrusions, distributed in the northern part as dike-like bodies along WNW trending faults, predominantly granite dikes with minor pegmatite and quartz veins. The principal mineral resources in the area are gold deposits. More than ten gold deposits and occurrences have been identified, including three active mines: Huanglong, Luming, and Bamiaoqou, and other prospects such as Jiudian, Shagou, Baisangyuan, Jindoupo, Gaojiaozhai, Jinwozi, and Changgou (Fig. 1b).

The mining area is predominantly underlain by the Lower Silurian Meiziya Formation (S_1m), composed of shallow-metamorphosed marine clastic rocks. This formation represents the principal gold-bearing stratigraphic unit in the region, resulting from greenschist-facies metamorphism of argillaceous–sandy sediments, and generally trends NWW-SEE. Based on lithology, mineral assemblages, and marker beds, the formation can be subdivided into six lithologic members. Among these, the first (S_1m_1) and second (S_1m_2) members are not exposed within the mining area. The third member (S_1m_3), distributed in the south-central part of the Huanglong gold deposit, consists mainly of sericite–quartz schist and two-mica quartz schist. The fourth member (S_1m_4), occurring in the central portion of the deposit, is composed of carbonaceous sericite–quartz schist and carbon-bearing meta-sandstone. The fifth member (S_1m_5), also located centrally, is in conformable contact with both the fourth and sixth members. It is further subdivided into two sub-layers, with the second sub-layer ($S_1m_5^2$) representing the major ore-hosting unit in the mining area. Thirteen gold orebodies identified to date are hosted within this sub-layer. The third

subunit ($S_1m_5^{2-3}$) primarily comprises carbonaceous sericite–quartz schist and carbonaceous biotite-porphyroblast sericite–quartz schist intercalated with thin layers of meta-sandstone. This subunit hosts the largest number of orebodies in the mining area, with nine orebodies discovered so far, including the G□ and G□ orebodies in the Jingou ore block, orebodies □, □-1, □-2, and □ in the Xiaohuangdong ore block, orebody KT2 in the Chayuan ore block, and orebodies KT6 and KT7 in the Wangjiawan ore block (Fig. 2). A series of fault fracture zones have developed within the brittle–ductile shear zones in the mining area. These faults generally trend NW, with associated minor folds, forming tight, recumbent, and other fold types along rheological boundaries between lithological units[14–15]. Magmatic activity in the mining area is weak, manifested only as minor granite dikes (10 m ~ 30 m long, 0.5 m ~ 2 m wide). Due to intense deformation in the region, these dikes commonly exhibit tectonic schistosity contacts with country rocks[16]. Wall-rock alteration near the orebodies is dominated by silicification, pyritization, pyrrhotitization, sericitization, chloritization, and biotite porphyroblast formation.

The Huanglong gold deposit comprises five ore blocks: Jingou, Xiaohuangdong, Wangjiawan, Shuidigou, and Chayuangou. The gold orebodies are primarily hosted within the Lower Silurian Meiziya Formation (S_1m). In the Wangjiawan block, Orebody KT7 is subdivided into four subsidiary orebodies: KT7-1, KT7-2, KT7-3, and KT7-4, all of which occur in the third subunit (S_1m5^{2-3}) of the second sub-layer of the fifth lithologic member of the Meiziya Formation. The host rock consists of carbonaceous biotite-porphyroblast sericite-quartz schist intercalated with carbon-bearing meta-sandstone. The orebodies strike for 50 m ~ 172 m, with thicknesses ranging from 0.72 m to 4.52 m and an average thickness of 1.95 m. The gold grade varies from a minimum of 0.37 g/t to a maximum of 21.38 g/t, averaging 2.17 g/t, characterizing a low-grade gold deposit (Fig. 3). Based on biotite porphyroblast size, the carbonaceous biotite-porphyroblast sericite-quartz schist ores are classified into three types: fine-grained (0.1 mm ~ 1 mm) (Fig. 4a), medium-grained (1 mm ~ 3 mm) (Fig. 4b), and coarse-grained (> 3 mm) (Fig. 4c). Backscattered electron imaging reveals that fine-grained ores contain metallic minerals dominated by pyrrhotite, arsenopyrite, chalcopyrite, and magnetite. Arsenopyrite exhibits euhedral to subhedral textures (Fig. 4d, g). Medium-grained ores contain gudmundite and arsenopyrite, along with the non-metallic mineral garnet. Arsenopyrite displays subhedral to anhedral, often fragmented, morphologies (Fig. 4e, h). Pyrrhotite in both fine- and medium-grained ores shows smooth and intact surfaces. In contrast, coarse-grained ores contain pyrrhotite, arsenopyrite, chalcopyrite, ilmenite, and the non-metallic minerals monazite and garnet. Pyrrhotite in these ores is characterized by abundant pores and fractures, with anhedral arsenopyrite inclusions. The variation in arsenopyrite crystal habit and the microtextural features of pyrrhotite suggest that increasing biotite porphyroblast size correlates with enhanced metamorphic intensity and greater mineral fragmentation. The presence of garnet indicates that metamorphic grade progressed from low- to medium-grade conditions (Fig. 4f, i).

Methods

For this study, six ore samples comprising two each of carbonaceous fine, medium, and coarse-grained biotite porphyroblast sericite quartz schist were collected from Orebody KT7 for observation and analysis. Petrographic thin-section observations were conducted at the Xi'an Mineral Resources Survey Center, China Geological Survey. The preparation of polished probe sections was performed by the Rock and Mineral Testing Center of the Hebei Institute of Geological Surveying and Mapping. Backscattered electron (BSE) imaging and electron probe microanalysis (EPMA) of sulfides were carried out at the Laboratory of Metallogenesis and Dynamics, Chang'an University.

Quantitative chemical analysis and BSE imaging of polished sections were performed using a JEOL JXA-8100 electron probe microanalyzer, targeting 16 elements. Operating conditions included an accelerating voltage of 15 kV, a beam current of 20 nA, and a focused beam diameter of 5.0 μm.

Discussion

EPMA Analysis

Electron probe microanalysis was conducted on arsenopyrite from carbonaceous sericite-quartz schist ores with fine, medium, and coarse-grained biotite porphyroblasts in Orebody KT7. The results are summarized in Table 1.

Arsenopyrite in fine-grained biotite-porphyroblast sericite-quartz schist (Apy1) exhibits euhedral to subhedral textures. Among 15 analytical points, Au contents above detection limits were recorded in 6 points, ranging from 0.01% to 0.15%, with an average of 0.09%. Arsenic varies between 45.13% and 46.68% (avg. 46.02%), S between 19.43% and 20.40% (avg. 19.9%), and Fe between 29.19% and 34.21% (avg. 31.70%). Cobalt ranges from 0.98% to 5.89% (avg. 3.62%), and Ni from 0.04% to 0.81% (avg. 0.21%). Elements such as Pb, Zn, Ag, Cu, and Te occur in low abundances, with Pb below detection limits. The structural formula of arsenopyrite is $As_{32.84–35.1}Fe_{29.86–33.39}S_{33.74–35.31}$.

Arsenopyrite in medium-grained biotite-porphyroblast sericite-quartz schist (Apy2) shows subhedral to anhedral textures. Three out of five points yielded detectable Au contents between 0.04% and 0.20% (avg. 0.11%). Arsenic ranges from 45.28% to 46.21% (avg. 45.80%), S from 19.64% to 20.70% (avg. 20.10%), and Fe from 29.81% to 34.58% (avg. 33.41%). Cobalt contents vary between 0.21% and 2.99% (avg. 0.99%), and Ni between 0.06% and 1.37% (avg. 0.34%). Trace elements including Pb, Zn, Ag, Cu, and Te are present in low concentrations. The empirical formula is $Fe_{30.39–33.36}As_{32.33–34.72}S_{33.32–34.89}$.

Table 1
Results of electron probe analysis of poisoned sand in carbonaceous biotite porphyritic sericulite schist ore of Huanglong Gold Deposit /%.

Point	Ore-hosting country rock	*W*(B)/%													
		As	Au	Sb	S	Fe	Pb	Co	Ag	Ni	Te	Cu	Zn	Total	Structural form
Apy1-1	Fine-grained biotite-porphyroblast ore	46.10	0.12	—	19.64	31.53	—	2.85	0.01	0.06	—	—	—	100.32	$Fe_{31.5}As_{34.33}S$
Apy1-2		45.99	—	—	20.40	33.71	—	2.33	—	0.13	—	—	—	102.54	$Fe_{32.56}As_{33.12}S$
Apy1-3		45.87	0.13	—	19.43	29.55	—	5.38	—	0.12	—	0.02	0.01	100.52	$Fe_{30.28}As_{35.04}S$
Apy1-4		46.22	—	—	19.98	29.67	0.09	5.04	—	0.81	0.02	—	—	101.84	$Fe_{29.99}As_{34.83}S$
Apy1-5		46.55	—	—	19.82	29.65	0.08	5.62	0.02	0.23	0.05	—	—	102.01	$Fe_{29.99}As_{35.1}S$
Apy1-6		46.04	0.08	—	19.98	33.39	—	2.27	—	0.04	—	0.13	—	101.92	$Fe_{32.57}As_{33.48}S$
Apy1-7		46.29	—	—	19.99	33.88	0.04	1.84	—	0.04	—	0.04	0.04	102.15	$Fe_{32.83}As_{33.43}S$
Apy1-8		45.67	—	—	19.81	29.19	—	5.89	0.02	0.32	0.03	—	—	100.93	$Fe_{29.86}As_{34.83}S$
Apy1-9		45.59	—	—	19.79	31.08	—	4.04	0.02	0.62	0.02	—	0.09	101.25	$Fe_{31.22}As_{34.14}S$
Apy1-10		45.13	—	—	19.86	34.21	0.05	0.98	0.01	—	0.01	0.04	0.11	100.40	$Fe_{33.39}As_{32.84}S$
Apy1-11		45.79	—	—	19.86	33.77	0.16	1.36	—	—	—	—	0.01	100.95	$Fe_{32.94}As_{33.3}S$
Apy1-12		45.72	0.15	—	19.86	32.21	0.10	3.36	0.03	0.05	—	0.04	—	101.50	$Fe_{31.93}As_{33.78}S$
Apy1-13		46.68	0.02	—	19.88	30.73	—	5.17	0.02	0.12	0.03	—	—	102.65	$Fe_{30.68}As_{34.74}S$
Apy1-14		46.32	0.01	—	20.31	32.05	—	3.91	—	0.06	0.01	0.01	0.10	102.77	$Fe_{31.43}As_{33.86}S$
Apy1-15		46.32	—	—	19.91	30.96	—	4.19	—	0.09	0.02	1.22	0.05	102.75	$Fe_{30.91}As_{34.47}S$
Apy2-1	Medium-grained biotite-porphyroblast ore	46.21	—	—	20.30	34.10	0.12	0.41	—	0.07	—	0.02	—	101.22	$Fe_{32.82}As_{33.15}S$
Apy2-2		45.28	0.20	—	20.70	34.58	0.06	0.33	—	0.07	0.01	0.02	—	101.26	$Fe_{33.12}As_{32.33}S$
Apy2-3		45.89	0.09	—	19.64	34.25	—	0.99	—	0.06	—	—	—	100.92	$Fe_{33.36}As_{33.32}S$
Apy2-4		45.69	0.04	0.10	19.64	29.81	0.07	2.99	0.02	1.37	0.01	—	—	99.74	$Fe_{30.39}As_{34.72}S$
Apy2-5		45.93	—	0.02	20.24	34.32	0.12	0.21	0.02	0.13	—	0.06	0.03	101.06	$Fe_{33.06}As_{32.98}S$
Apy3-1	Coarse-grained biotite-porphyroblast ore	45.62	0.01	—	20.21	32.65	0.06	1.45	0.02	0.04	0.04	0.01	—	100.11	$Fe_{32.05}As_{33.39}S$
Apy3-2		45.62	—	—	20.12	33.05	0.15	0.99	—	0.09	0.01	—	0.05	100.07	$Fe_{32.36}As_{33.31}S$

Arsenopyrite in coarse-grained biotite-porphyroblast sericite-quartz schist (Apy3) is predominantly anhedral. One of two analytical points yielded Au content of 0.01%. Arsenic averages 45.80%, S ranges from 20.12% to 20.21% (avg. 20.17%), and Fe from 32.65% to 33.05% (avg. 32.85%). Cobalt varies between 0.99% and 1.45% (avg. 1.22%), Ni between 0.04% and 0.09% (avg. 0.06%), Pb between 0.06% and 0.15% (avg. 0.10%), and Te between 0.01% and 0.04% (avg. 0.02%). Zinc, Ag, and Cu occur in minor amounts. The calculated formula corresponds to $Fe_{32.05–32.36}As_{33.34–33.39}S_{34.33–34.56}$.

Characteristics of Gold-Host Minerals and Occurrence of Gold

In carbonaceous porphyroblastic sericite-quartz schist ores, arsenopyrite is primarily associated with gudmundite. The morphology of arsenopyrite varies with the grain size of the biotite porphyroblasts: it is predominantly euhedral to subhedral in fine-grained biotite porphyroblasts (Apy1), subhedral to anhedral in medium-grained ones (Apy2), and mainly anhedral in coarse-grained varieties (Apy3). EPMA results indicate that Au contents at some analysis points

exceed detection limits, but its distribution is heterogeneous, suggesting the presence of localized Au enrichment. However, no native gold particles were observed under scanning electron microscopy, implying that Au primarily occurs as "invisible gold" within the arsenopyrite.

Correlations among As, S, Fe, and Au in the gold-bearing arsenopyrite are shown in Fig. 5. A weak correlation between Au and Fe (Fig. 5a) suggests no inherent genetic link between them. In contrast, Au exhibits a linear negative correlation with both S and As (Fig. 5b, c), indicating that Au may occur via isomorphic substitution for S or As (e.g., Au^{+} replacing S^{2-} or As^{3+}).

Studying the occurrence of gold provides direct evidence for understanding gold mineralization processes and is crucial for deciphering the metallogenesis of gold deposits. Based on particle size, gold can be classified as visible gold (> 0.2 mm), microscopic gold (0.2 μm ~ 0.2 mm), and submicroscopic gold (< 0.2 μm). Visible and microscopic gold are generally observable, whereas submicroscopic gold is typically "invisible"[17–18]. Previous studies on finely disseminated gold deposits have summarized that gold mainly resides in sulfides (such as arsenian pyrite, pyrrhotite, and arsenopyrite), with minor amounts in clay minerals and quartz[19–20]. Research has identified two principal forms of gold in sulfides[21–22]: (1) chemically bound gold, where Au enters the sulfide lattice as lattice-bound Au[23–25], and (2) gold occurring as discrete mineral inclusions. The solubility limit of Au in arsenian pyrite has been empirically approximated by the linear relationship $C_{Au} = 0.02C_{As} + 4\times10^{-5}$, where C_{Au} and C_{As} represent the molar fractions of Au and As, respectively[26–27]. In a lgAs-lgAu diagram (Fig. 5d), data points plotting above this solubility limit line suggest the presence of nanoparticulate native gold (Au^{0}), whereas those below the line indicate gold likely occurs in solid solution (Au^{+}).

In this study, EPMA data were converted to molar concentrations and plotted in Fig. 5d. All analytical points for arsenopyrite fall below the gold saturation curve, indicating that gold in these arsenopyrite samples likely exists predominantly in the form of solid solution (Au^{+}).

Arsenopyrite Formation Conditions

Kretschmar[28] first proposed using the Fe-As-S mineral assemblages and their chemical compositions to determine arsenopyrite formation temperature and sulfur fugacity, based on its low solubility and high sensitivity to temperature. This approach was later refined by Sharp[29], and the arsenopyrite geothermometer has since been widely applied in studies of various hydrothermal deposits[30–31].

In the Huanglong gold deposit, the principal gold-host minerals in carbonaceous biotite-porphyroblast sericite-quartz schist ores are arsenopyrite and pyrrhotite. By plotting the atomic percentage of As in arsenopyrite within the Fe-As-S phase diagram, key physicochemical parameters of arsenopyrite formation were constrained (Fig. 6). The estimated temperatures for arsenopyrite range from 360℃ to 475℃, indicating a high-temperature regime. For context, Jiao[32] applied the Holdaway garnet-biotite geothermometer in the adjacent Tiefosi area and obtained metamorphic temperatures of 490℃~610℃. Gao[5] calculated garnet-biotite temperatures of 590℃~670℃ for the Jindoupo gold deposit. Yang[4] used EPMA data and phase equilibrium constraints for pyrrhotite from the Huanglong deposit to estimate a formation temperature of 230℃~250℃. Previous fluid inclusion studies from regional gold deposits suggest mineralization temperatures of 170℃~300℃, consistent with a meso to epithermal origin[3]. Feng[33] proposed that regional ductile nappe structures in northern Ankang formed at temperatures > 450℃, whereas ore-controlling ductile shear zones experienced deformation at < 350℃, with the most favorable conditions for gold deposition occurring around 200℃.

The formation temperature of arsenopyrite can be constrained using sulfide assemblages and its As atomic content[8]. In this study, arsenopyrite in fine-grained biotite-porphyroblast ore (Apy1) has an As atomic percentage of 32.84%~35.10%, corresponding to a formation temperature of 390℃~475℃ and $lgf(S_2)$ values of − 9.7 to − 6.6. Medium-grained biotite-porphyroblast ore (Apy2) contains arsenopyrite with 32.33%~34.72% As, yielding temperatures of 360℃~460℃ and $lgf(S_2)$ of − 10.5 to − 7.2. Coarse-grained biotite-porphyroblast ore (Apy3) shows As contents of 33.31%~33.39%, with corresponding temperatures of 410℃~415℃ and $lgf(S_2)$ of − 9.0 to − 8.9. Overall, increasing biotite porphyroblast size correlates with decreasing sulfur fugacity and arsenopyrite formation temperature.

Microscopic observations indicate a mineral paragenesis in the order of biotite and garnet, followed by arsenopyrite, then pyrrhotite. As arsenopyrite formed at progressively lower temperatures, pyrrhotite became increasingly fractured and porous-features indicative of decompressive boiling. This process led to a drop in sulfur fugacity within the hydrothermal system, triggering the breakdown of Au complexes and subsequent gold precipitation. This interpretation is consistent with the observed negative correlation between Au and S in arsenopyrite..

Genetic Model of the Deposit

During the Indosinian orogeny, regional geosynclinal closure initiated metamorphism and compressional thrusting, leading to the formation of metamorphic minerals such as biotite. The Late Indosinian to Early Yanshanian period represented a critical metallogenic epoch in the Qinling Orogenic Belt[34]. As the South Qinling entered an intracontinental orogenic stage, intense tectonic deformation further metamorphosed the rocks in the study area, generating a series of EW-trending brittle-ductile shear zones. These zones contained abundant fine fractures and cleavages, with S_1 foliation being progressively replaced by S_2. Subsequent stress release facilitated the development of structurally controlled decompression and dilation zones[35–36].

Concurrently, deep-seated magmatic activity intensified, driving rapid upward migration of heat and fluids. This induced thermal metamorphism, resulting in the crystallization of garnet and the coarsening of biotite into porphyroblasts. In strata with elevated background gold concentrations, gold was mobilized and transported as complexes along structural fractures. Changes in redox conditions eventually triggered gold precipitation within fractures and cleavage planes of the shear zones.

Furthermore, the crystallization of sulfide minerals progressively depleted sulfur ion concentrations in the hydrothermal fluid, destabilizing gold complexes and promoting their precipitation. This process led to the intimate association of gold with iron sulfides such as pyrrhotite and arsenopyrite, establishing these sulfides as the principal hosts of gold mineralization.

Results

(1) Arsenopyrite in fine-grained biotite porphyroblasts is predominantly euhedral to subhedral (Apy1), whereas in medium-grained varieties it is mainly subhedral to anhedral (Apy2), and in coarse-grained types it is primarily anhedral (Apy3). No native gold particles were observed via scanning electron microscopy, indicating that gold occurs predominantly as "invisible gold" within the arsenopyrite structure, likely through isomorphic substitution for S or As.

(2) Increasing biotite porphyroblast size correlates with decreasing sulfur fugacity and arsenopyrite formation temperature. The crystallization temperatures of arsenopyrite range from 360℃ to 475℃, indicative of a high-temperature regime, with corresponding sulfur fugacity ($\lg f(S_2)$) values between − 10.5 and − 6.6.

(3) The porous and fractured morphology of the sulfides exhibits characteristics of decompressive boiling. This process led to a decrease in sulfur fugacity within the hydrothermal system, triggering the decomposition of gold complexes and subsequent precipitation. This interpretation is consistent with the negative correlation observed between Au and S in arsenopyrite.

Declarations

Competing interests

The authors declare no competing interests.

Funding Declaration

This work was supported by the China Geological Survey under Project [2025]02-064-03, Survey and Evaluation of Gold-Polymetallic Deposits in Muerzekelede (K43E021020), Halajun Township, Kizilsu Kirghiz Autonomous Prefecture, Xinjiang (Project Identity Code: DD20230206403).

Author Contribution

Conceptualization, Zhongkai Xue and Haoqing Huang; Acquired funding, Zhongkai Xue and Baocheng Fan; Methodology, Zhongkai Xue, Shukai Li, Anmin Xu and Xin Zheng; Formal analysis, Zhongkai Xue, Baocheng Fan, Hang Li and You Guo; Investigation, Haoqing Huang and Datong Liu; Resources, Zhongkai Xue; Writing—original draft preparation, Zhongkai Xue; Writing—review and editing, Haoqing Huang; Visualization, Zhongkai Xue; Supervision, Haoqing Huang. All the authors have read and agreed to the published version of the manuscript.

Acknowledgements

The authors acknowledge with thanks the helpful comments, suggestions and a constructive critique of the manuscript by the reviewers and Editor, Scientific Reports.The authors Thanks for the funding and support provided by the project (DD20230206403) of the China Geological Survey.

Data Availability

All data generated or analysed during this study are included in this published article.

References

1. Han, K., Yang, X., An, L., et al. S_2 foliation characteristics of brittle-ductile shear zone in the Huanglong gold deposit, Hanyin, South Qinling and its effect on mineralization. *Northwestern Geology*, **51**, 171-184(2018).
2. Tan, L., Yang, B., Liu, X., et al. Material source and metallogenic model of gold deposit in Huanglong, Shaanxi Province. *Mineral Exploration*, **12**, 549-556(2021).
3. Cui, W. Discussion on geological characteristics, source of ore forming material and genesis of Huanglong gold deposit in Hanyin, Shaanxi Province. *Chang'an University*, (2023).
4. Yang, H., Yang, H., Yang., et al. Typomorphic mineralogy and gold-bearing property of pyrrhotite in Huanglong gold deposit, Southern Qinling Mountains. *Geology and Resources*, **28**, 246-253(2019).
5. Gao, Y., Yang, X., Han, K., et al. Study on S_2 foliation, Condition of temperature-pressure on biotite-garnet metacryst minerals and the relation of ore-control in Jindoupo ore area of the Northern Hanyin, South Qinling. *Journal of Earth Sciences and Environment*, **38**, 464-472(2016).
6. Morey, A., Tomkins, A., Bierlein, F., et al. Bimodal distribution of gold in pyrite and arsenopyrite: Examples from the Archean Boorara and Bardoc shear systems, Yilgarn craton, Western Australia. *Economic Geology*, **103**, 599-614(2008).

7. Zoheir, B., Goldfarb, R., Holzheid, A., et al. Geochemical and geochronological characteristics of the Um Rusgranite intrusion and associated gold deposit, Eastern Desert, Egypt. *Geoscience. Frontier*, **11**, 325-345(2020).
8. Lu, H., Zhu, X., Shan, Q., et al. Hydrothermal evolution of gold-bearing pyrite and arsenopyrite from different types of gold deposits. *Mineral Deposits*, **32**, 823-842(2013).
9. Pan, M., Hu, K., Cao, J., et al. Gold-bearing Characteristics of Arsenian Pyrites and Arsenopyrites in the Bojitian Carlin-type Gold Deposits, Southwestern Guizhou Province, Southwest China. *Geological Journal of China Universities*, **19**, 293-306(2013).
10. Hou, L., Peng, H., Ding, J., et al. Textures and in situ chemical and isotopic analyses of pyrite, Huijiabao trend, Youjiang basin, China: Implications for paragenesis and source of sulfur. *Economic Geology*, **111**, 331-353(2016).
11. Chen, M., Mao, J., Chen, Z., et al. Mineralogy of arsenian pyrites and arsenopyrites of Carlin-type gold deposits in Yunnan-Guizhou-Guangxi “golden triangle” area southwestern China. *Mineral Deposits*, **28**, 539-557(2009).
12. Chen, C., Zhang, Y., Gu, X., et al. Modes of occurrence of gold in arsenopyrite from Miaolong gold deposit in Sandu，Guizhou Province. *Mineral Deposits*, **32**, 932-940(2013).
13. Zhang, G., Zhang, Z., Dong, Y. Nature of main tectono-lithostratigraphic Units of the Qinling Orogen: Impliations for the tectonic evolution. *Acta Petrologica Sinica*, **11**, 101-114(1995).
14. Zhao, J., Liu, H., Li, H. Geological characteristics of gold fields in northern Hanyin County, Shanxi Province. *Scientific and Technological Information*, **19**, 432-433(2013).
15. Du, J. Discussion on the geological characteristics and prospecting potential of Silurian gold-bearing deposit in north Ankang. *China Mine Engineering*, **43**, 39-43(2014).
16. Zang, J., Chen, G., Wang, J., et al. Geology of gold deposits in Northern Ankang-Shiquan, Shanxi Province. *Geology of Shanxi*, **31**, 47-52(2013).
17. Cook, N., Chryssoulis, S. Concentrations of invisible gold in the common sulfides. *The Canadian Mineralogist*, **28**, 1-16(1990).
18. Xu, W., Niu, N., Zhang, M. Study on the occurrence state of gold in Jiashan gold-copper mining area, Liaoning. *Gold*, **32**, 18-21(2011).
19. Wu, X. Study on the occurence of gold and its specific technological property in Lan-Ni-Gou Gold Mine. *Gold*, **13**, 11-16(1992).
20. Liu, J., Xia, Y., Deng, Y., et al. Re-study on modes of gold occurrence in the Shuiyindong super-large-sized gold deposit. *Guizhou Geology*, **24**, 165-169(2007).
21. Simon, G., Kesler, S., Chryssoulis, S. Geochemistry and textures of gold-bearing arsenianpyrite Twin Creeks Nevada :Implications for deposition of gold in Carlin-type deposit. *Economic Geology* **94**, 405-422(1999).
22. Reich, M., Kesler, S., Utunomiya, S., et al. Solubility of gold in arsenian pyrite. *Geochimica et Cosmochimica Acta*. **69**, 2781-2796(2005).
23. Arehart, G., Chryssoulis, S., Kesler, S. Gold and arsenic in iron sulfides from sediment-hosted disseminated gold deposits: Implications for depositional processes. *Economic Geology*, **88**, 171-185(1993).
24. Fleet, M., Mumin, A. Gold-bearing arsenian pyrite and marcasite and arsenopyrite from Carlin Trend gold deposits and laboratory synthesis. *American Mineralogist*, **82**, 182-193(1997).
25. Palenik, C., Utsunomiya, S., Reich, M., et al. "Invisible" gold revealed: Direct imaging of gold nanoparticles in a Carlin-type deposit. *American Mineralogist*, **89**, 1359-1366(2004).
26. Radtke, A., Heropoulos, C., Fabbi, B., et al. Data on major and minor elements in host rocks and ores, Carlin gold deposit, Nevada. *Economic Geology*, **67**, 975-978(1972).
27. Sun, Z., Liu, Y. Electron microscope study on the analysis of ultramicroscopic gold in Carlin-type gold deposits. *Journal of electron microscopy*, **2**, 186(1993).
28. Kretschmar, U., Scott, S. Phase relations involving arsenopyrite in the system Fe-As-S and their application. *Mineral*, **14**, 364-386(1976).
29. Sharp, Z., Essene, E., Kelly, W. A re-examination of the arsenopyrite geothermometer: Pressure considerations and applications to natural assemblages. *Mineral*, **23**, 517-534(1985).
30. Zhang, B., Li, N., Shu, S., et al. Textural and compositional evolution of Au-hosting Fe-S-As minerals at the Axi epithermal gold deposit, Western Tianshan, NW China. *Ore Geology Review*, **100**, 31-50(2018).
31. Liu, J., Kou, S., Wang, Z., et al. Genesis of Xinjiazui Gold Deposit: In Situ Geochemical Constraints from Arsenopyrite. *Mineral*, **14**, 1031-1050(2024).
32. Jiao, J., Yang, X., Chou, D. Lithofacies mapping of Silurian structure and metallogenic regularity of gold deposits in Shiquan County, Shanxi Province. *Chang’an University*(2014).
33. Feng, M., Yang, J. Basic characteristic of ductile nappe structure and its ore-contral of gold deposit in North Ankang. *Geology of Shanxi*, **12**, 17-26(1994).
34. Mao, J., Zhou, Z., Feng, C., et al. A preliminary study of the Triassic large-scale mineralization in China and its geodynamic setting. *Geology in China*, **39**, 1437-1471(2012).
35. Yang, X., Han, K., Wu, X., et al. Structural deformation characteristics and evolution of the intracontinental orogeny in South Qinling: Analysis of Late Indosinian-Yanshanian structural deformation in the Shiquan-northern Hanyin area. *Earth Science Frontiers*, **23**, 72-80(2016).
36. Yang, X., He, H., Chao, H., et al. A comparative study of magmatic core complexes and metamorphic core complexes with case studies of ore-controlling: Structural assemblages and ore-controlling models of the Niushan–Fenghuangshan metamorphic core complex and the northern Niushan magmatic core complex, South Qinling. *Geological Bulletin of China*, **42**, 520-539(2023).

Figures

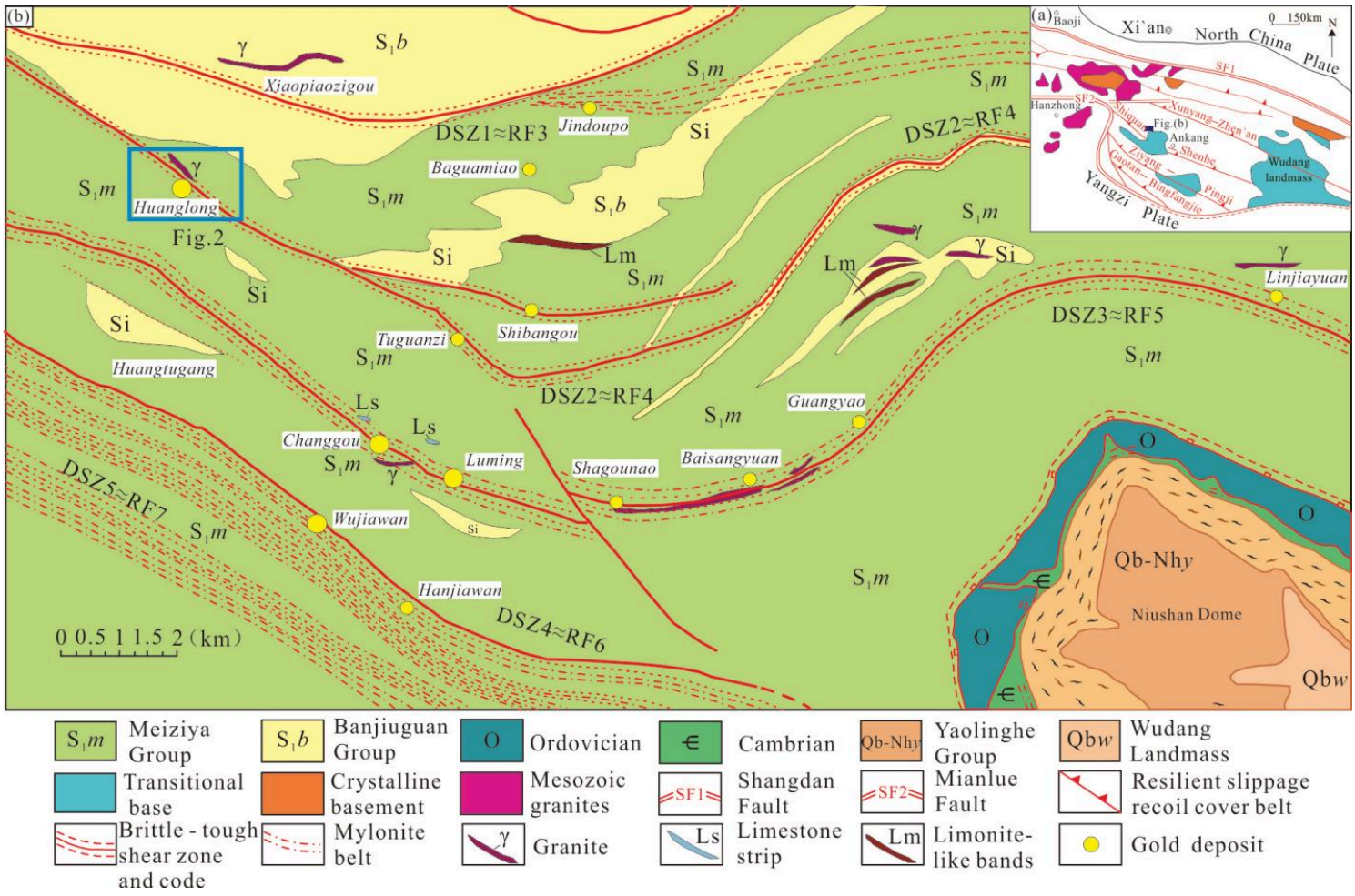


Figure 1

Tectonic Location Map (a) and Geological Simplified Map (b) of the northern part of Hanyin in the South Qinling Mountains (modified after Cui et al.[3]).

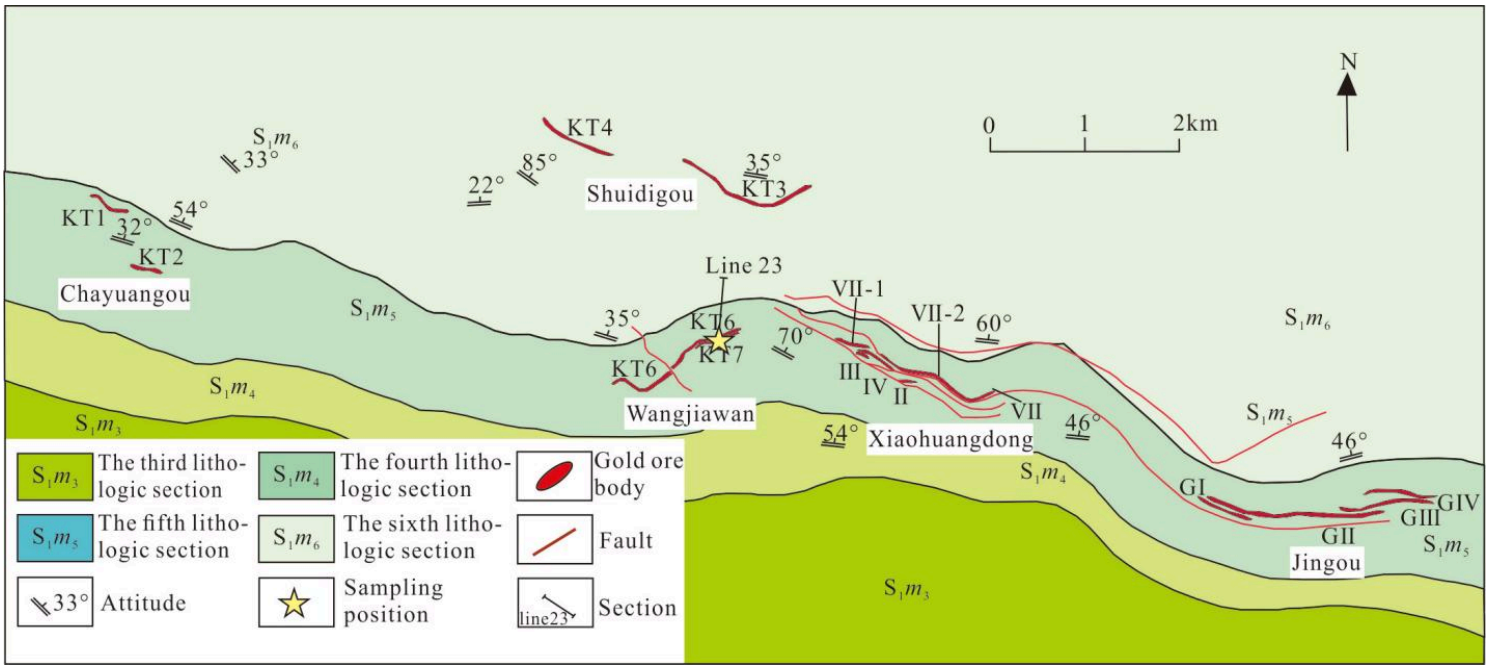


Figure 2

Geological Simplified map of Huanglong Mining Area (modified after Han et al.[1]).

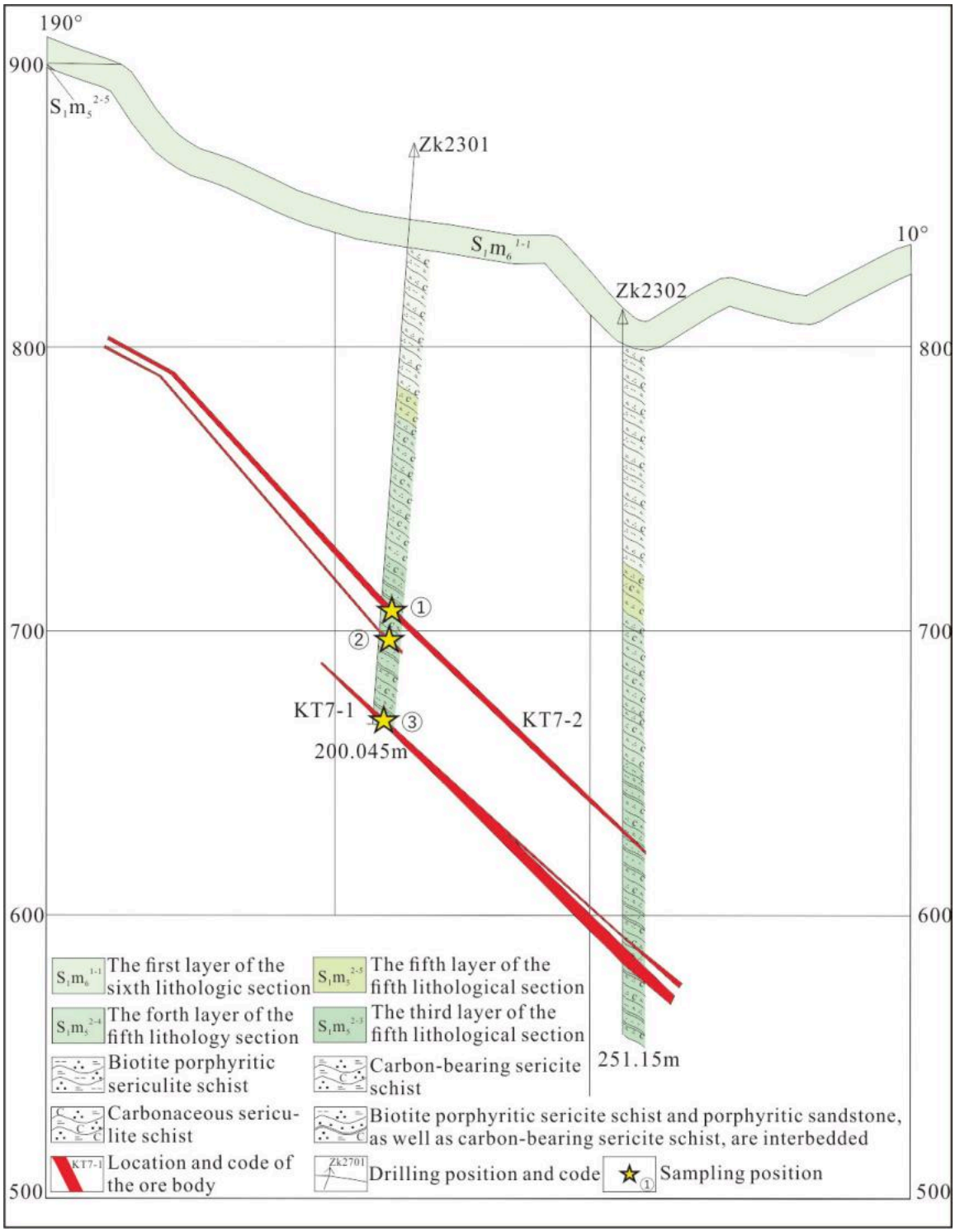


Figure 3

Cross-sectional view of Exploration Line 23 of Huanglong Gold Deposit.

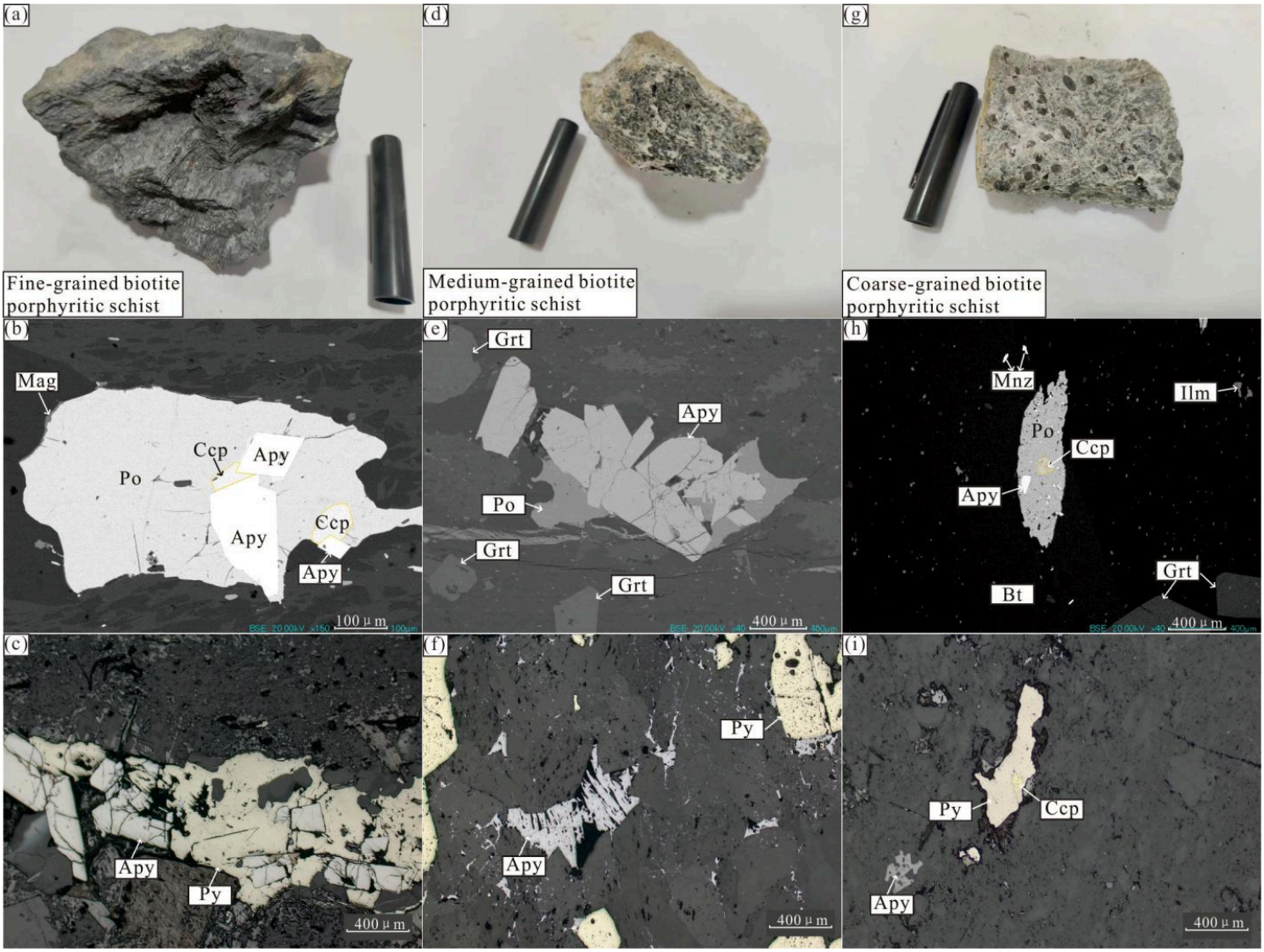


Figure 4

Hand specimens and BSE images of the Huanglong gold deposit.

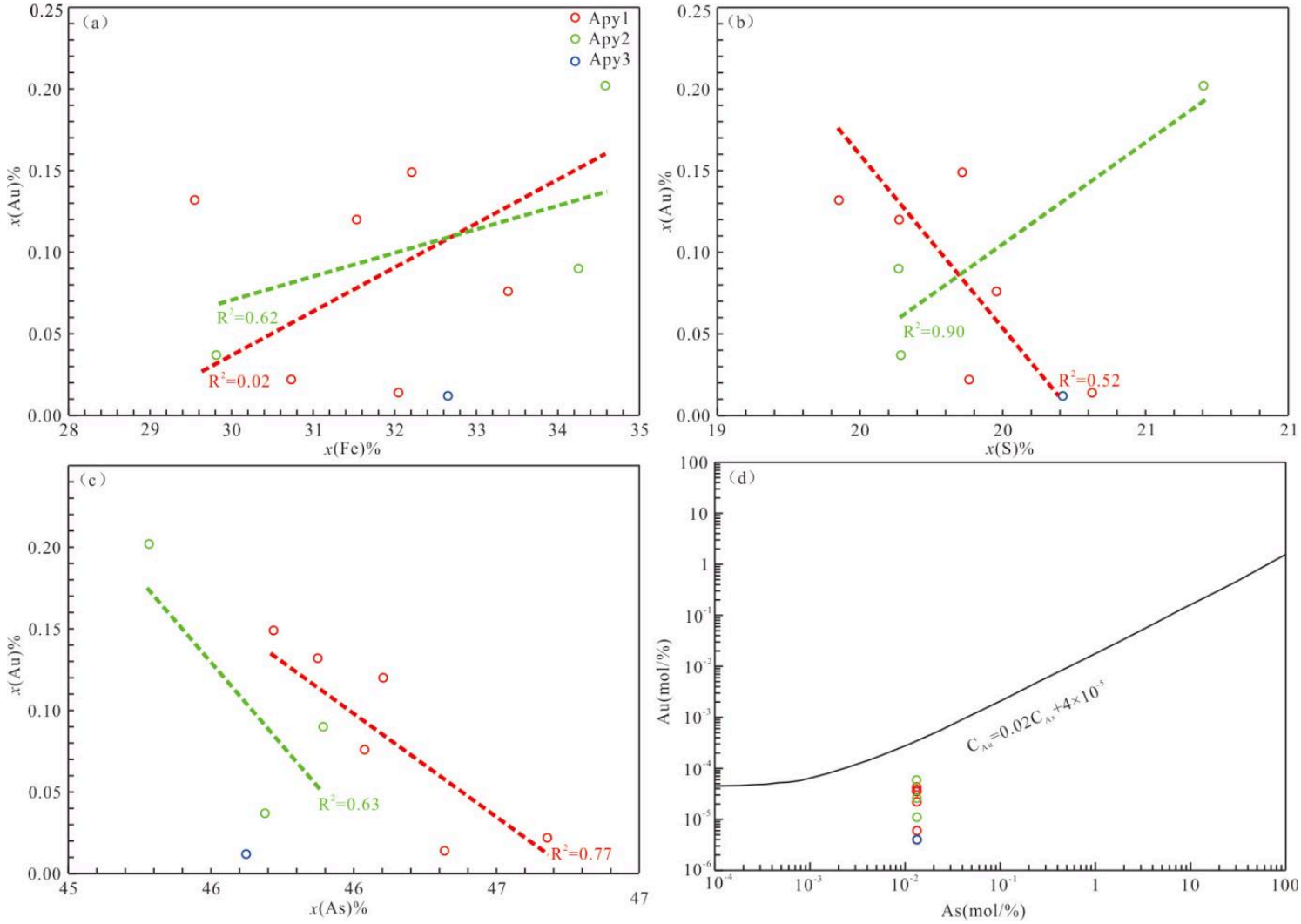


Figure 5

Correlation diagram of toxic sand As-S, Au-As and Fe-Au in the Huanglong Gold Deposit (modified after Reich et al.[22]).

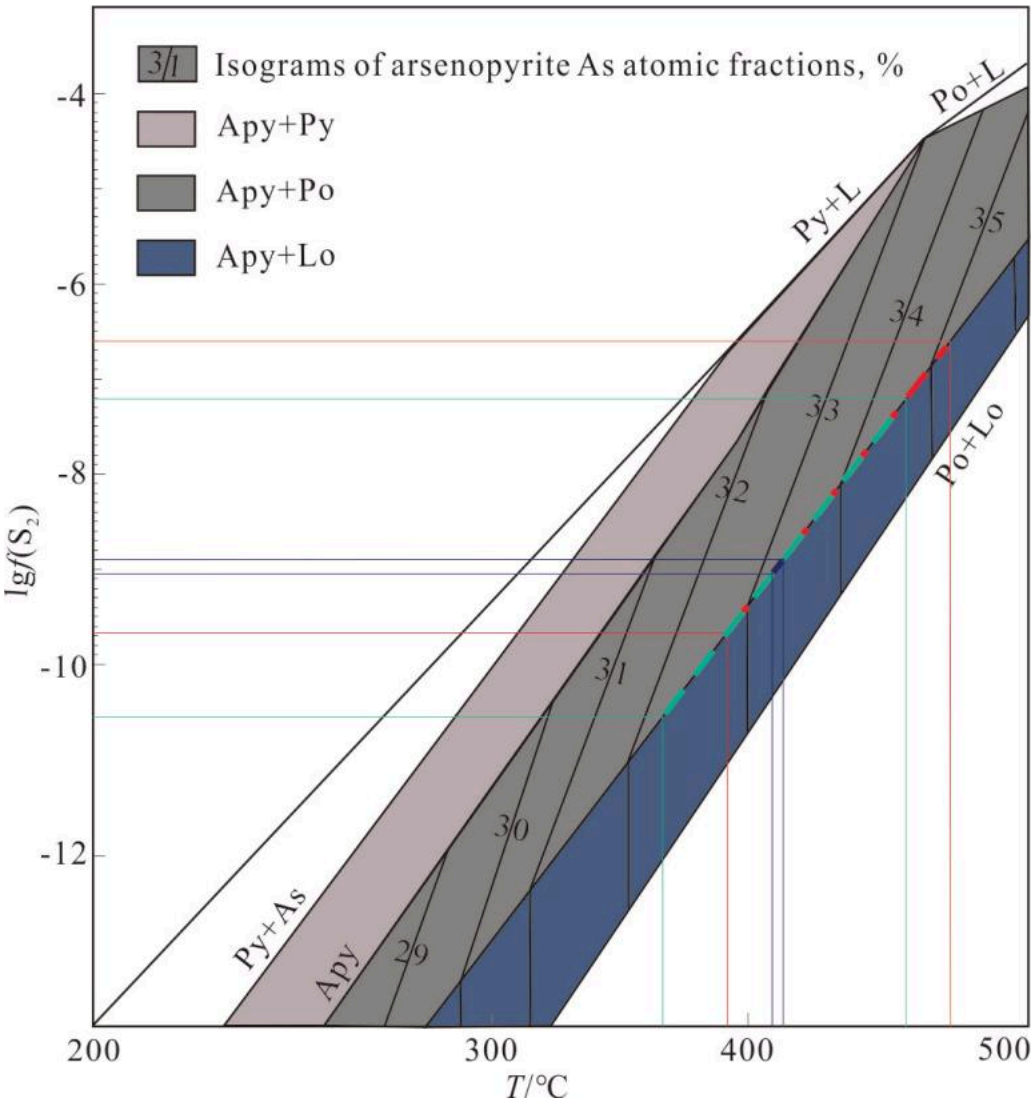


Figure 6

Balance diagram of lg$f$(S_2) (sulfur fugability) and T (°C) of the toxic sand geological thermometer (modified after Sharp et al.[29] and Zhang et al.[30]).